Polymer 109 (2017) 85–92

Contents lists available at ScienceDirect

Polymer

journal homepage: www.elsevier.com/locate/polymer

# Evaluating the influence of heteroatoms on the electronic properties of aryl[3,4-*c*]pyrroledione based copolymers

Benjamin J. Hale [a], Moneim Elshobaki [b, c], Ryan Gebhardt [b], David Wheeler [d], Jon Stoffer [a], Aimée Tomlinson [d], Sumit Chaudhary [b, e], Malika Jeffries-EL [a, *]

[a] Department of Chemistry, Iowa State University, Ames, IA 50011, United States
[b] Department of Materials & Science Engineering, Iowa State University, Ames, IA 50011, United States
[c] Department of Physics, Mansoura University, Mansoura 35516, Egypt
[d] Department of Chemistry & Biochemistry, University of North Georgia, Dahlonega, GA 30597, United States
[e] Department of Electrical and Computer Engineering, Iowa State University, Ames, IA 50011, United States

ARTICLE INFO

*Article history:*
Received 13 September 2016
Received in revised form
29 November 2016
Accepted 3 December 2016
Available online 6 December 2016

*Keywords:*
Conjugated polymer
Organic semiconductors
Donor-acceptor
Copolymers

ABSTRACT

A donor-acceptor-type conjugated copolymer (PBDT-PPD) composed of benzodithiophene (BDT) and pyrrolopyrroledione (PPD) was synthesized using the Stille cross-coupling reaction. Using both experimental and theoretical data, the optical, electrochemical, and photovoltaic properties of PBDT-PPD were compared with those of its sulfur analog, PBDT-TPD, which is composed of BDT and thienopyrroledione (TPD). The optical bandgaps of the polymers were determined to be 1.86 and 2.20 eV, respectively. While both materials possessed similar highest occupied molecular orbital (HOMO) levels, the lowest unoccupied molecular orbital (LUMO) level for PBDT-PPD was raised relative to that of PBDT-TPD. Devices incorporating PBDT-PPD had a higher open-circuit voltage and fill factor, yet drastically lower short-circuit current density ($J_{sc}$) than PBDT-TPD leading to a lower power conversion efficiency (PCE). The lack of significant intramolecular charge transfer (ICT) combined with the high LUMO of PBDT-PPD resulted in poor spectral overlap with the solar spectrum, lowering $J_{sc}$. Additionally, there was poor electron injection into PCBM, which also reduced the PCE.



## 1. Introduction

Since the discovery of the first semiconducting polymer nearly 40 years ago, research involving conjugated polymers has been on the rise. In particular, studies involving bulk hetero-junction (BHJ) organic photovoltaic solar cells (OPVs), has increased exponentially due to their potential low cost production, and use in lightweight, flexible devices [1–9]. Although improvements in materials and fabrication techniques have led to dramatic increases in OPV performance, as determined by the power conversion efficiency (PCE), a better understanding of structure-property relationships is still desired [10,11]. The synthesis of conjugated polymers, comprised of alternating π-electron rich and π-electron deficient arylene units, allows for the selective tuning of optical and electronic properties of the material [12–14]. This "donor-acceptor" strategy has given rise to a variety of materials with desirable properties, such as broad optical absorption bands, deep HOMO energy levels, high charge carrier mobilities, and LUMO levels with appropriate alignment to [6,6]-phenyl-$C_{71}$-butyric acid methyl ester ($PC_{71}BM$) [8,15]. In addition, these materials can be further tuned by varying the heteroatoms within the arenes. Indeed, a dramatic impact on the physical, optical, and electronic properties of a material can be achieved through heteroatom substitution [8,16]. For example, large changes in optical absorption and solubility of many materials have been observed upon replacing of thiophene with the isoelectronic furan or selenophene [16–19]. While substitution within a group (e.g. the group 16 chalcogens) can at often times have predictable effects, the impact of substitution between groups is often less straightforward [16,20,21].

The thiophene containing 5-octylthieno[3,4-*c*]pyrrole-4,6-dione (TPD) unit has been used as an π-electron deficient moiety in a variety of high efficiency donor-acceptor copolymers [22–24]. When polymerized with the π-electron rich benzodithiophene (BDT), BHJ OPV performance as high as 5.5% for 1.0 $cm^2$ devices (PBDT-TPD) has been reported [22]. When the thiophene was

* Corresponding author.
*E-mail address:* malikaj@bu.edu (M. Jeffries-EL).

http://dx.doi.org/10.1016/j.polymer.2016.12.013
0032-3861/

replaced with furan (FPD), a widening of the optical bandgap was observed, whereas switching with selenophene (SePD) resulted in a reduction of the optical bandgap, relative to TPD [25]. OPVs fabricated from the SePD based polymer showed a greatly reduced short-circuit current density ($J_{sc}$), which resulted in a very low PCE of 0.26% [26]. Although an improvement in performance has not been seen with FPD or SePD, exploration outside of the group 16 elements has yet to be researched extensively.

A seldom studied alternative to TPD is the nitrogen analog pyrrolo[3,4-*c*]pyrroledione (PPD), first reported in 1996 [27]. While, the additional alkyl chain on the nitrogen atom of PPD can potentially increase solubility, the impact of replacing sulfur with nitrogen is not well understood. Recently, PPD was used in a series of donor-acceptor copolymers with varying results, and there was no direct structural comparison to known high performing TPD based materials [28]. Here, a PPD based copolymer was synthesized, characterized and compared to the structurally analogous PBDT-TPD. In addition to the physical methods, we also evaluated both polymers through density functional theory.

## 2. Results and discussion

### 2.1. Synthesis and characterization of monomer and polymers

The PPD monomer **6** was prepared according the synthetic route as illustrated in Scheme 1 [27]. Diethyl pyrrole-3,4-dicarboxlyate was formed by condensation of diethyl fumarate and *p*-toluenesulfonylmethyl isocyanide followed by saponification to the dicarboxylic acid, **2**. Compound **2** was then converted to the corresponding anhydride by treatment with *N,N′*-dicyclohexylcarbodiimide, which was ring opened with *n*-octylamine, and closed with thionyl chloride to give **4**. The unalkylated **4** was then brominated using NBS in the dark. Compound **5** was then alkylated, in a fashion similar to its structural isomer diketopyrrolopyrrole, in DMF with potassium carbonate, 1-bromooctane, and 18-crown-6 to give the final PPD monomer, **6**, in moderate yield.

Alternating copolymers were synthesized by Stille cross-coupling of the diarylhalide monomers (PPD or TPD) and the distannyl BDT monomer in anhydrous toluene, as shown in Scheme 2. The molecular weight data for **PBDT-TPD** and **PBDT-PPD** were determined by size exclusion chromatography in chloroform against polystyrene standards. Both materials had reasonable number averaged molecular weights ($M_n$) of 24.9 and 19.8 kDa for **PBDT-TPD** and **PBDT-PPD**, respectively. The TPD based polymer, **PBDT-TPD**, had poor solubility in organic solvents at room temperature, but was readily dissolved in chlorobenzene and 1,2-dichlorobenzene when heated, as reported by Leclerc et al. [22] The PPD based polymer, **PBDT-PPD**, had greatly improved solubility and was readily dissolved in chloroform, chlorobenzene, and 1,2-dichlorobenzene at room temperature. The increased solubility of **PBDT-PPD** is likely due to the lower degree of polymerization ($DP_n$) and the additional solubilizing alkyl chain on the nitrogen.

The thermal stabilities of the polymers were evaluated using TGA under air (Supporting Information). **PBDT-TPD** and **PBDT-PPD** demonstrated good thermal stability when heated, with a 5% weight loss at 333 and 337 °C, respectively. Differential scanning calorimetry (Supporting Information) revealed no phase transitions for **PBDT-PPD** below 250 °C. The molecular weights and thermal properties of **PBDT-TPD** and **PBDT-PPD** are summarized in Table 1.

### 2.2. Optical and electrochemical properties

The optical properties of the polymers were investigated using UV-Vis absorption spectroscopy. The normalized absorption spectra of the polymers, both as dilute chloroform solutions and thin films on glass substrates, are shown in Figs. 1 and 2, respectively. **PBDT-TPD** had a broad absorption from 350 to 650 nm in dilute solution with two peaks of nearly equal intensity at 552 and 627 nm, with a third slightly smaller peak at ~590 nm. The intensities of the broad low energy transition suggests intramolecular charge-transfer (ICT) interaction between the electron-rich BDT and the electron-deficient TPD moieties [29]. In solution **PBDT-PPD** displayed a $\lambda_{max}$ of 526 nm with a narrower and significantly blue shifted absorption range of 350–550 nm, relative to **PBDT-TPD**. Strong vibronic coupling can be seen in **PBDT-PPD** and **PBDT-TPD**, suggesting the formation of aggregates in both solutions.

As a thin film, **PBDT-TPD** showed very little change in absorption when compared to its solution spectra, with a $\lambda_{max}$ of 624 nm. A slight decrease in the intensity of the higher energy maximum and an increase in the intensity of vibronic coupling was also seen, with the vibronic coupling indicating highly ordered thin films [30]. Interestingly, the thin film of **PBDT-PPD**, had a $\lambda_{max}$ of 533 nm, with a reduction in intensity, and a significant narrowing of the absorption range by a decrease of the $\pi$-$\pi^*$ transitions of the conjugated main chain. A comparison of the absorption profiles of the two polymers shows **PBDT-TPD** has a stronger absorption across nearly all wavelengths, relative to their respective $\lambda_{max}$, and a significantly broader absorption of 350–675 nm, versus the 350–550 nm range of **PBDT-PPD**. The optical bandgaps were determined from the absorption onsets of the polymer films. The measured optical bandgaps for **PBDT-TPD** and **PBDT-PPD** were 1.86 eV and 2.20 eV, respectively. The narrow absorption range of **PBDT-PPD** and the wide bandgap suggest there is little, if any, ICT occurring between the BDT and PPD moieties [31–33]. The optical data is summarized in Table 2.

Cyclic voltammetry was used to investigate the redox behavior and to estimate the HOMO energy levels of the polymers. The HOMO and LUMO energy levels were calculated from the oxidation onset using the adjusted energy level of ferrocene/ferrocenium ($Fc/Fc^+$) as −4.7 eV vs vacuum and are summarized in Table 2. Both polymers exhibited reversible reduction and irreversible oxidation peaks (Supporting Information). The HOMO energy level for both **PBDT-TPD** and **PBDT-PPD** were found to be −5.50 eV, while the LUMO energy levels were found to be −3.54 eV and −3.10 eV, for **PBDT-TPD** and **PBDT-PPD** respectively. The electrochemical bandgaps of 1.96 eV for **PBDT-TPD** and 2.40 eV for **PBDT-PPD** are in agreement with the optical bandgaps [34]. While both materials had the same HOMO level, the significantly higher LUMO level and narrowing of the optical absorption of PBDT-PPD reinforce the suspicion that there is little intramolecular charge transfer along the polymer backbone. To further investigate this possibility, Density functional theory (DFT) calculations were performed.

### 2.3. Computational studies

DFT was used to evaluate the differences in the performance between **PBDT-TPD** and **PBDT-PPD**. We began with the B3LYP (Becke, three-parameter, Lee-Yang-Parr) [35] hybrid functional which has been shown to produce comparable geometries to Moller-Plesset second-order perturbation theory (a higher level of theory) [36] at a fraction of the computational cost [37]. Although, the improved performance of OPVs based **PBDT-TPD** can be attributed to the smaller band gap and a lower lying LUMO level relative to **PBDT-PPD**, other factors may be involved. Upon completion of the DFT calculations, the frontier molecular orbitals (FMOs) and electrostatic potential maps were generated (Fig. 3). For **PBDT-TPD**, the terminal TPD ring appears to be lacking electron density in the HOMO, whereas its LUMO is rich in electron density. The opposite trend occurs for the terminal BDT ring within **PBDT-TPD**, in which the HOMO is rich in electron density and the LUMO is

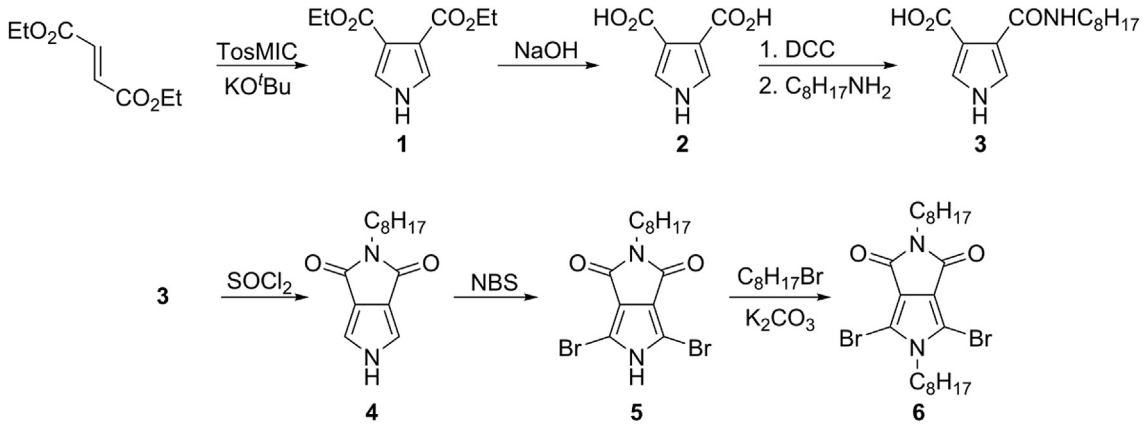


**Scheme 1.** Synthesis of PPD monomer **6**.

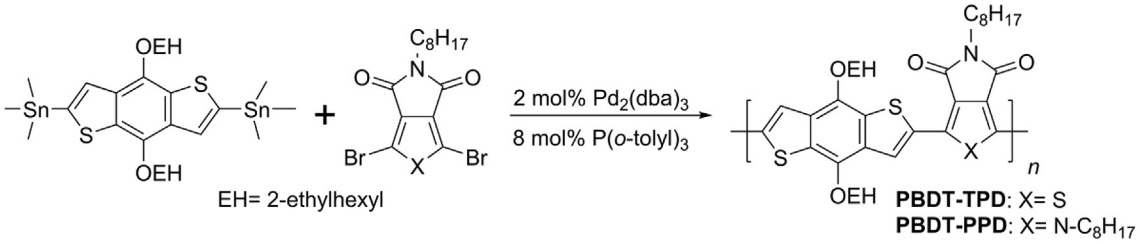


**Scheme 2.** Synthesis of donor-acceptor copolymers **PBDT-TPD** and **PBDT-PPD**.

**Table 1**
Molecular weight and thermal properties of the synthesized polymers.

| Polymer | Yield[a] (%) | $M_n$[b] (kDa) | $M_w$[b] (kDa) | Đ[c] | $DP_n$ | $T_d$5%[d] (°C) |
|---|---|---|---|---|---|---|
| PBDT-TPD | 82 | 24.9 | 44.8 | 1.8 | 35.1 | 333.7 |
| PBDT-PPD | 73 | 19.8 | 33.6 | 1.7 | 24.6 | 337.8 |

[a] Isolated yield.
[b] Determined by GPC vs polystyrene standards in chloroform.
[c] Dispersity: $M_w/M_n$.
[d] Temperature at 5% weight loss with a heating rate of 20 °C $min^{-1}$ under air.

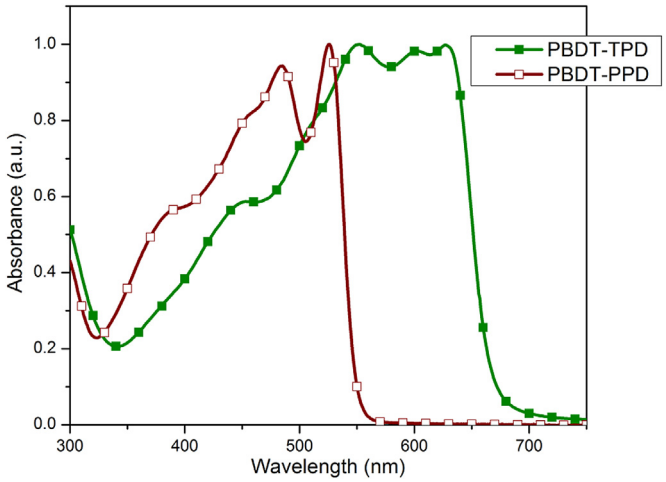


**Fig. 1.** Normalized UV-Vis spectra of **PBDT-TPD** and **PBDT-PPD** in $CHCl_3$.

lacking in electron density. Additionally, both TPD rings show a lack of electron density in the HOMO-1, whereas these rings are electron

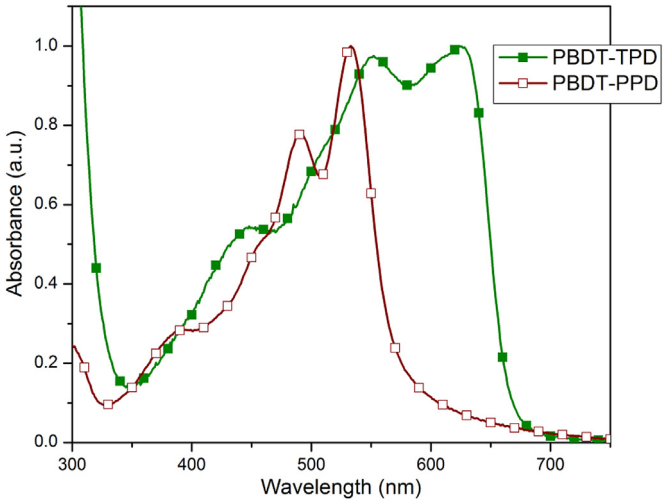


**Fig. 2.** Normalized UV-Vis spectra of **PBDT-TPD** and **PBDT-PPD** thin films.

rich in the LUMO+1. Collectively, these findings indicate that there is donor-acceptor behavior within **PBDT-TPD**.

However this was not the case for **PBDT-PPD** as the both PPD rings have electron density in the HOMO and the LUMO. Furthermore, there is complete lack of electron density on the PPD moiety in the HOMO-1 and an absence of electron density in the LUMO+1 of the terminal PPD unit. Thus donor-acceptor behavior alone was not enough to explain the observed difference. We then turned our attention to the geometry of the dimers. This data indicated that the **PBDT-TPD** system was nearly planar with dihedral angles ranging from 177 to 180°. On the other hand, the **PBDT-PPD** was non-planar with dihedrals angles ranging from 146 to 151°. This

twist can be seen in the electrostatic potential map and also adversely effects the distribution of electron density seen in the FMOs. The lack of planarity is also responsible for raising the HOMO and the LUMO and increasing the band gap. Collectively, these factors result in the poor performance of **PBDT-PPD**.

A comparison between the experimental electrochemical results and the theoretical data is shown in Table 3. An absolute difference of 0.35 eV and 0.22 eV was found in the HOMO and band gap respectively, indicating there is good agreement between the two data sets. In order evaluate the potential for charge transfer within these copolymers the reorganization energy for both the hole and the electron was computed and shown in Table 4. This energy was generated for both the individual subunits as well as the comonomer in each case. In the case of **PBDT-TPD**, the BDT subunit had a much lower reorganization energy for electron than for the hole indicating it takes less energy for this ring to accept a negative charge than it does for a positive charge. The opposite is true for TPD in which the hole reorganization energy is lower than that of the electron. Putting the two subunits together and making a comonomer shows that the material behaves more favorably as an acceptor than a donor. For the **PBDT-PPD** copolymer, the PPD is more accepting than donating in nature as indicated by the reorganization energy. Like **PBDT-TPD, PBDT-PPD** is an also electron-accepting material. Overall, all of these reorganization energies are quite high and so while trends can be suggested based on their magnitude it is doubtful either of these copolymers would be able to charge-transfer at a reasonable rate.

### 2.4. Photovoltaic properties

Photovoltaic devices were fabricated with the structure ITO/PEDOT:PSS/donor:$PC_{71}BM$/Ca/Al, where ITO is indium tin oxide and PEDOT:PSS is poly(3,4-ethylenedioxythiophene)-poly(-styrenesulfonate). Characteristic $J$–$V$ curves are shown in Fig. 4 and the resulting data is summarized in Table 5. Solutions were cast from a 25 mg $mL^{-1}$ total blend concentration in chlorobenzene using a ratio of 1:2 polymer:$PC_{71}BM$ w/w. Spin-rates ranging from 1000 rpm to 1400 rpm were examined. The best devices of **PBDT-TPD** gave a PCE of 2.5%, with an open-circuit voltage ($V_{OC}$) of 0.68 V, a short-circuit current density ($J_{SC}$) of 7.98 mA $cm^{-2}$, and a fill factor (FF) of 46%, while the best devices of **PBDT-PPD** gave a significantly lower PCE of 0.63%, $V_{OC}$ of 0.87 V, $J_{SC}$ 1.3 mA $cm^{-2}$, and a FF of 57%.

In an effort to further improve the poor performance of **PBDT-PPD**, devices were fabricated with the use of small quantities of the high boiling solvent additives 1-chloronaphthalene (CN) and 1,8-diiodooctane (DIO) at 5% v/v. In general, devices made from solution with additives had higher PCE in comparison to the ones without additives. Devices fabricated using CN as an additive gave a maximum PCE of 0.83%, an average PCE of 0.72%, $V_{OC}$ of 0.66 V, $J_{SC}$ of 2.5 mA $cm^{-2}$, but a greatly reduced FF of 44%. The devices using DIO gave a significantly higher maximum PCE of 1.34% and an average of 1.23%, $V_{OC}$ of 0.76 V, $J_{SC}$ of 3.9 mA $cm^{-2}$, but also had a low FF of 42%.

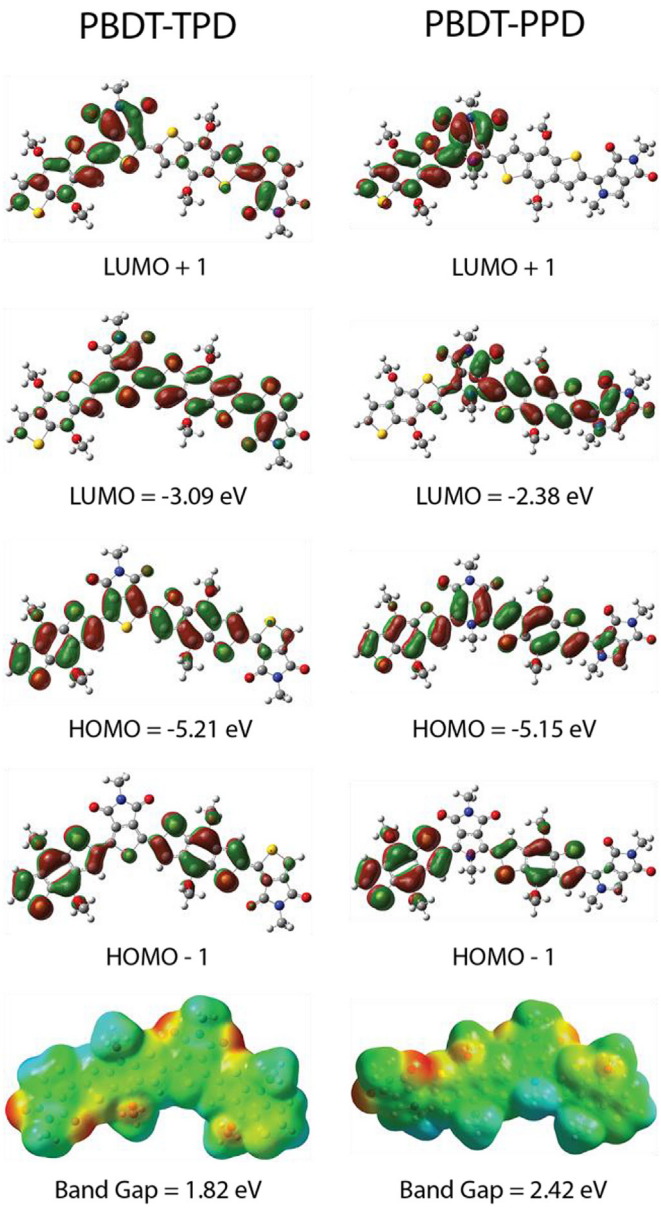


**Fig. 3.** DFT calculated frontier orbital and electrostatic potential maps.

While improvement was observed using solvent additives, the overall photocurrent remained very low.

The surface roughness and phase distribution of the polymers were studied by atomic force microscopy (AFM) (Fig. 4). The AFM roughness maps of PBDT-TPD:$PC_{70}BM$ and PBDT-PPD:$PC_{70}BM$ neat thin-films show large domain sizes with root-mean square surface

**Table 2**
Optical and electrochemical properties of the synthesized polymers.

| Polymer | $\lambda_{max}^{soln}$ (nm)[a] | $\lambda_{max}^{film}$ (nm) | $E_g^{opt}$ (eV)[b] | $E_{HOMO}$ (eV)[c] | $E_{LUMO}$ (eV)[d] | $E_g^{EC}$[e] (eV) |
|---|---|---|---|---|---|---|
| PBDT-TPD | 552, 627 | 624 | 1.86 | −5.50 | −3.54 | 1.96 |
| PBDT-PPD | 526 | 533 | 2.20 | −5.50 | −3.10 | 2.40 |

[a] Measured in chloroform.
[b] Measured from the optical onset.
[c] HOMO $= -(E_{onset}^{ox} + 4.7)$eV.
[d] LUMO $= -(E_{onset}^{red} - 4.7)$eV.
[e] $E_g^{EC}$ = LUMO − HOMO.

roughness (RMS) values of 3.99 and 5.17 nm, respectively. Whereas the AFM height images reveal smooth topography for both polymers with root-mean square (RMS) surface roughness values less than 1.30 nm. The $J_{SC}$ of the **PBDT-PPD** device increased from 1.3 mA cm$^{-2}$ to 3.9 and 2.5 mA cm$^{-2}$ upon using as solvent additives of DIO and CN, respectively. This enhancement in $J_{SC}$ is a result of the reduction in the domain size within the morphology of PBDT-PPD-based thin-films with solvent additives as seen in AFM images (Figs. 5 and 6). The films with additives have small grain sizes with slight variation in the surface roughness ($RMS_{DIO}$ = 5.59 nm, and $RMS_{CN}$ = 4.25 nm). This morphological change is beneficial for suppressing the charge recombination and better charge transport and dissociation is achieved.

The hole mobilities of **PBDT-TPD** and **PBDT-PPD** were examined using the space-charge limited current (SCLC) method with a hole only device structure of ITO/PEDOT:PSS/polymer:$PC_{71}BM$/$MoO_x$/Al. The mobilities were calculated according to the equation:

$$J_{SCLC} = \frac{9}{8}\varepsilon_o \varepsilon_r \mu_h \left(V^2 / L^3\right), \quad (1)$$

where $\varepsilon_o$ is the permittivity of vacuum, $\varepsilon_r$ is the permittivity of the material, $\mu_h$ is the carrier mobility, $V$ is the effective voltage, and $L$ is the thickness of the active layer. The hole mobilities were determined to be 4.36 × 10$^{-6}$ for **PBDT-TPD** and 1.31 × 10$^{-5}$ cm$^2$ V$^{-1}$ s$^{-1}$ for **PBDT-PPD**. The hole-only current-voltage characteristics are shown in Fig. 7.

Since the **PBDT-PPD** blend has a higher mobility and more favorable morphology than the **PBDT-TPD** blend, one of the most likely causes for the low photocurrent of **PBDT-PPD** is the absorption profile of the material having poor overlap with the solar spectrum [30]. Additionally, the high LUMO of **PBDT-PPD** may have too high of an offset with that of $PC_{71}BM$, leading to recombination in the donor due to the poor rate of electron injection into the acceptor [31].

## 3. Conclusions

A novel conjugated polymer, **PBDT-PPD** was synthesized and compared to the well-known sulfur analog **PBDT-TPD**. Both polymers were used in OPVs and it was found that **PBDT-PPD** performed worse than **PBDT-TPD**. Experimental and theoretical studies on the optoelectronic properties of these polymers demonstrated that **PBDT-PPD** had a lower electron affinity and wider optical bandgap than **PBDT-TPD**. Furthermore, the ICT was weaker in **PBDT-PPD** than in **PBDT-TPD**, and neither material was a particularly good donor polymer. Collectively, these results suggest that replacing sulfur with nitrogen in pyrrole dione monomers could be a good strategy for designing efficient OPV materials, however a different electron-donating group should be explored. Research is ongoing in our group to improve upon these results.

**Table 3**
Comparison between theoretical and experimental values.

| | HOMO (eV) | | | LUMO (eV) | | | Bandgap (eV) | | |
|---|---|---|---|---|---|---|---|---|---|
| | DFT | Expt | Diff | DFT | Expt | Diff | DFT | Expt | Diff |
| **PBDT-TPD** | −5.21 | −5.50 | 0.29 | −3.09 | −3.54 | 0.45 | 1.82 | 1.86 | 0.04 |
| **PBDT-PPD** | −5.15 | −5.50 | 0.35 | −2.38 | −3.10 | 0.72 | 2.42 | 2.20 | 0.22 |

**Table 4**
Reorganization energies (in eV) for the subunits and their monomers.

| | BDT | PPD | TPD | PBDT-TPD | PBDT-PPD |
|---|---|---|---|---|---|
| $\lambda_h$[a] | 0.838 | 0.399 | 0.400 | 0.762 | 0.798 |
| $\lambda_e$[b] | 0.337 | 0.478 | 0.476 | 0.414 | 0.445 |

[a] Hole reorganization: $\lambda_h$.
[b] Electron reorganization: $\lambda_e$.

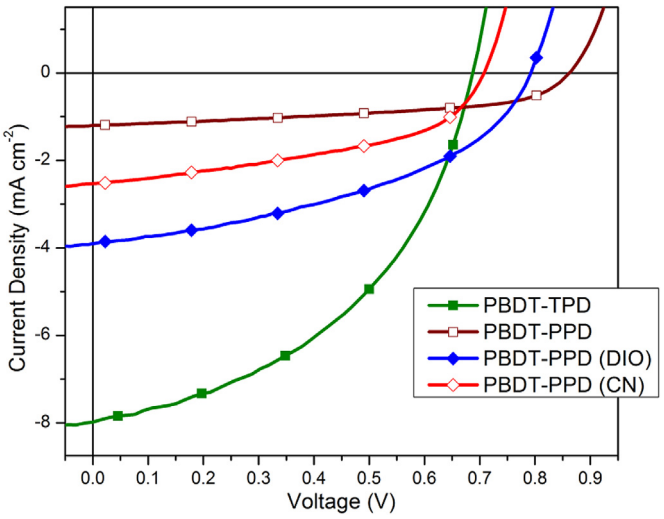


**Fig. 4.** *J–V* curves of PBDT-TPD and PBDT-PPD photovoltaic devices.

**Table 5**
Summary of the characteristics of photovoltaic devices.

| Polymer[a] | Additive[b] | $J_{SC}$ (mA cm$^{-2}$) | $V_{OC}$ (V) | FF (%) | $PCE_{ave}$[e] (%) | $PCE_{max}$ (%) |
|---|---|---|---|---|---|---|
| PBDT-TPD | – | 7.8 | 0.69 | 45 | 2.44 | 2.51 |
| PBDT-PPD | – | 1.3 | 0.87 | 52 | 0.59 | 0.63 |
| | DIO[c] | 3.9 | 0.76 | 42 | 1.23 | 1.34 |
| | CN[d] | 2.5 | 0.66 | 44 | 0.72 | 0.83 |

[a] Fabricated at a 1:1.5 weight ratio of polymer:$PC_{71}BM$ with a total solution concentration of 25 mg mL$^{-1}$.
[b] 5% *v/v*.
[c] 1,8-diiodooctane.
[d] 1-chloronaphthalene.
[e] Average of six devices.

## 4. Experimental

### 4.1. Materials

Air- and moisture-sensitive reactions were performed using standard Schlenk techniques. Solvents used for palladium-catalyzed reactions were deoxygenated prior to use by sparging with argon for 30 min. The preparation of compounds **6** and **8** are described in the Supporting Information. (4,8-bis((2-ethylhexyl)oxy)benzo[1,2-*b*:4,5-*b'*]dithiophene-2,6-diyl)bis(trimethylstannane) (BDT) [38] was prepared according to literature procedures. Thiophene-3,4-dicarboxylic acid was purchased from Oakwood Chemicals and recrystallized from water before use. All other chemical reagents were purchased commercially and used without further purification unless otherwise noted.

### 4.2. Characterization

Nuclear magnetic resonance (NMR) spectra were collected on

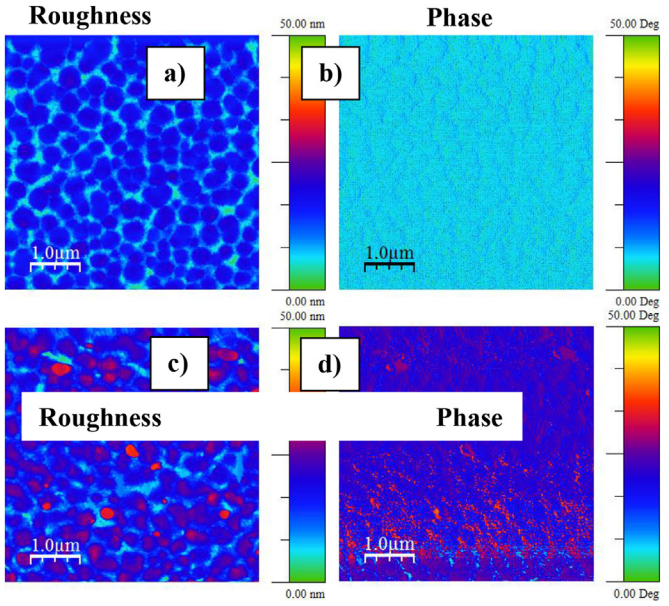


**Fig. 5.** AFM height (left) and phase (right) images at 5 μm × 5 μm of PBDT-TPD:$PC_{71}BM$ (a–b), PBDT-PPD:$PC_{71}BM$ (c–d) thin-films.

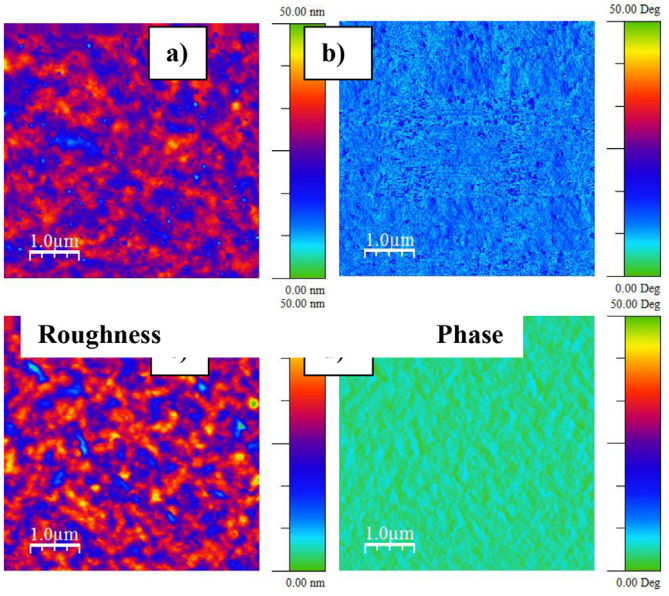


**Fig. 6.** AFM height (left) and phase (right) images at 5 μm × 5 μm of PBDT-PPD:$PC_{71}BM$ with 5% DIO (a–b) and 5% CN (c–d) solvent additives.

Varian VXR-300, Varian MR-400, or Bruker Advance III-600 spectrometers. $^1H$ NMR spectra were internally referenced to the residual solvent peak. In all spectra, chemical shifts are given in ppm ($\delta$) relative to the solvent. Gel permeation chromatography (GPC) measurements were performed on a Shimadzu Prominence GPC with two 10 μm AM Gel columns connected in series (guard, 10,000 Å, 1000 Å) in chloroform at 40 °C relative to polystyrene standards. Thermogravimetric analysis (TGA) were performed over an interval of 30–850 °C at a heating rate of 20 °C $min^{-1}$ under ambient atmosphere. Differential scanning calorimetry (DSC) was performed using a first scan heating rate of 15 °C $min^{-1}$ to erase thermal history and a second scan to measure transitions between 0 and 330 °C under nitrogen. Cyclic voltammetry (CV)

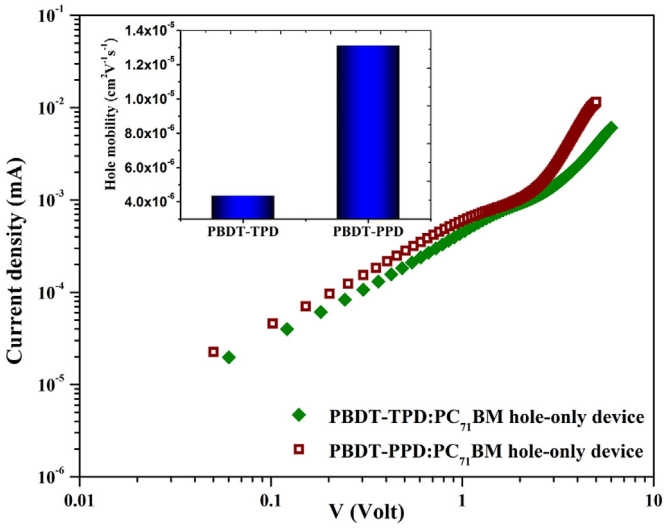


**Fig. 7.** The current-voltage characteristics of PBDT-TPD:$PC_{71}BM$ and PBDT-PPD:$PC_{71}BM$ photovoltaic devices in dark under ambient conditions.

measurements were carried out using an *e*-DAQ *e*-corder 410 potentiostat with a scanning rate of 100 mV $s^{-1}$. The polymer films were dropcast from 1–2 mg $mL^{-1}$ solutions in chlorobenzene onto a platinum working electrode. $Ag/Ag^+$ and Pt wire were used as the reference and auxiliary electrodes, respectively. The reported values were referenced to $Fc/Fc^+$ (−4.8 versus vacuum). All electrochemical experiments were performed in deoxygenated acetonitrile under an argon atmosphere using 0.1 M tetrabutylammonium hexafluorophosphate as electrolyte. Absorption spectra were obtained on a photodiode-array Agilent 8453 UV-visible spectrophotometer using polymer solutions in $CHCl_3$ and thin films. The films were cast by spin coating 25 × 25 × 1 mm glass slides using solutions of polymer (2.5–5.0 mg $mL^{-1}$) in $CHCl_3$/*o*-dichlorobenzene at a spin rate of 1200 rpm on a Headway Research, Inc. PWM32 spin-coater. A Veeco Digital Instruments atomic force microscope was used to capture the surface roughness and phase of PBDTTPD- and PBDTPPD-based thins films. The tapping-mode AFM was carried out using TESPA tip with scan rate of 0.6 μm $s^{-1}$ and scan size of 5 μm × 5 μm.

### 4.3. Computational modeling

To elucidate the difference in performance between **PBDT-TPD** and **PBDT-PPD** we performed theoretical calculations using density functional theory (DFT). The geometries of model oligomers (n = 1, 2, 3, and 4) for both copolymers were optimized at the B3LYP/6-31G* level in which the long side chains were truncated to methyl groups in order to save computational expense. The first ten excited states were determined through a time dependent density functional theory treatment using the same level of theory as the optimization. The HOMO, LUMO, and optical band gaps were produced by fitting the set of oligomers with the Kuhn expression: [39,40].

$$E = E_0\sqrt{1 + 2\frac{k'}{k_0}\cos\frac{\pi}{N+1}} \quad (2)$$

where $E_0$ is the transition energy of a formal double bond, N is the number of double bonds in the oligomer (thought to be identical oscillators), and $k'/k_0$ is an adjustable parameter (indicative of the strength of coupling between the oscillators). In addition, the

reorganization energy, which is a measure of charge mobility for both the hole ($\lambda_h$) and electron ($\lambda_e$), was calculated using: [41–44].

$$\lambda = (E_0^* - E_0) + (E_\pm^* - E_\pm) \quad (3)$$

where $E_0$ and $E_\pm$ are the energies of the neutral and charged optimized geometries and the $E_0^*$ and $E_{\pm 0}^*$ are the energies of neutral geometry with charge and the charged geometry set to neutral.

### 4.4. Fabrication of photovoltaic devices

All devices were produced via a solution-based, spin-casting fabrication process. All polymers were mixed with $PC_{70}BM$ (1-material) (mixed 1:1.5 with a total solution concentration of 25 mg $mL^{-1}$) dissolved in chlorobenzene (Sigma Aldrich) and stirred overnight at 115 °C at 800 rpm. ITO (sheet resistance: 5–15 $\Omega^{-1}$) coated glass slides (Delta Technologies) were cleaned by consecutive 10 min sonication in (i) Alconox detergent (dissolved in deionized water), (ii) deionized water, and then (iii) isopropanol. The slides were then dried with $N_2$ and cleaned with air plasma for 10 min. Filtered (0.45 μm) PEDOT:PSS (Clevios P™ 4083) was spin-coated onto the prepared substrates (5000 rpm/60 s) and then annealed at 120 °C for 20 min. After cooling, the substrates were transferred to an argon-filled glovebox. The polymer:$PC_{70}BM$ solutions were filtered with 0.2 μm pore filter, and simultaneously dropped onto the PEDOT:PSS-coated substrates and spin-cast at 1400 rpm for 60 s. The films were dried under petri-dish for 8 h. For the active layers with solvent additives, 5% (v/v) of either CN or DIO was added to the stock solution, and then deposited at the aforementioned casting conditions. Finally, Ca (20 nm) and Al (100 nm) were thermally evaporated through a shadow mask (area = 0.1256 $cm^{-2}$) under vacuum of $10^{-6}$ mbar to complete the devices. Current-voltage (*J-V*) data were generated by illuminating the devices using an ELH Quartzline halogen lamp at 1 sun. The solar simulator was calibrated using a crystalline silicon photodiode with a KG-5 filter. The hole only devices were prepared following the same procedure, except calcium was replaced with molybdenum suboxide. The hole mobility was extracted from the SCLC measurement using a Keithley 2400 SourceMeter in the dark under ambient conditions.

## 5. Synthesis

### 5.1. Synthesis of PBDT-TPD

BDT (193.0 mg, 0.25 mmol) and compound **8** (105.7 mg, 0.25 mmol) were dissolved in toluene (9 mL) and sparged with argon for 30 min. Tris(dibenzylideneacetone)dipalladium(0) (4.9 mg, 2 mol%) and tri(*o*-tolyl)phosphine (7.1 mg, 9 mol%) were added and the reaction refluxed for 48 h. The polymer was end-capped by refluxing with trimethyl(phenyl)tin (50 mg) for 4 h, followed by refluxing with iodobenzene (0.1 mL) overnight. After cooling to ambient temperature, the mixture was precipitated into methanol and filtered through a Soxhlet thimble. The polymer was washed with methanol (4 h), acetone (4 h), hexanes (12 h), and extracted with chloroform. The chloroform fraction was then concentrated and the polymer run through a short silica gel plug. The resulting fraction was then concentrated (~5 mL) and precipitated into methanol, filtered, and dried to give the expected polymer as a dark purple solid (145.6 mg, 82%). $M_n$: 24.9 kDa, PDI: 1.8; Not soluble enough in $CDCl_3$ for $^1H$ NMR.

### 5.2. Synthesis of PBDT-PPD

Compound **6** (186.2 mg, 0.36 mmol) and BDT (278.0 mg, 0.36 mmol) were dissolved in toluene (10 mL) and sparged with argon for 30 min. Tris(dibenzylideneacetone)dipalladium(0) (6.6 mg, 2 mol%) and tri(*o*-tolyl)phosphine (9.8 mg, 9 mol%) were added and the reaction refluxed for 48 h. The polymer was end-capped by refluxing with trimethyl(phenyl)tin (50 mg) for 4 h, followed by refluxing with iodobenzene (0.1 mL) overnight. After cooling to ambient temperature, the mixture was precipitated into methanol and filtered through a Soxhlet thimble. The polymer was washed with methanol (4 h), acetone (4 h), hexanes (12 h), and extracted with chloroform. The chloroform fraction was then concentrated and the polymer run through a short silica gel plug. The resulting fraction was then concentrated (~5 mL) and precipitated into methanol, filtered, and dried in vacuo to give the expected polymer as a dark orange solid (210.8 mg, 73%). $M_n$: 20.1 kDa, PDI: 1.8; $^1H$ NMR (600 MHz, $CDCl_3$) $\delta$ 8.34 (s, 2H), 4.63 (s, 2H), 4.40 (s, 4H), 3.64 (s, 2H), 2.05–0.68 (m, 60H).

## Funding

This work was supported by the 3M Foundation and Iowa State University (ISU) and partially supported by DMR-1410088.

## Acknowledgements

We wish to thank Steve Veysey and the ISU Chemical Instrumentation Facility for training and assistance with the thermal analysis. We also thank Dr. Kamel Harrata and the ISU Mass Spectroscopy Laboratory for analysis. The OPVs were fabricated at the ISU Microelectronics Research Center.

## Appendix A. Supplementary data

Supplementary data related to this article can be found at http://dx.doi.org/10.1016/j.polymer.2016.12.013.

## References

[1] H. Shirakawa, E.J. Louis, A.G. Macdiarmid, C.K. Chiang, A.J. Heeger, Synthesis of electrically conducting organic polymers - halogen derivatives of polyacetylene, (Ch)X, J. Chem. Soc. Chem. Comm. 16 (1977) 578–580.
[2] C.K. Chiang, C.R. Fincher, Y.W. Park, A.J. Heeger, H. Shirakawa, E.J. Louis, S.C. Gau, A.G. MacDiarmid, Electrical conductivity in doped polyacetylene, Phys. Rev. Lett. 39 (17) (1977) 1098–1101.
[3] S.B. Darling, F. You, The case for organic photovoltaics, RSC Adv. 3 (39) (2013) 17633–17648.
[4] A. Facchetti, π-conjugated polymers for organic electronics and photovoltaic cell applications†, Chem. Mat. 23 (3) (2010) 733–758.
[5] B.C. Thompson, J.M.J. Fréchet, Polymer–Fullerene composite Solar cells, Angew. Chem. Int. Ed. 47 (1) (2008) 58–77.
[6] G. Yu, J. Gao, J.C. Hummelen, F. Wudl, A.J. Heeger, Polymer photovoltaic cells: enhanced efficiencies via a network of internal donor-acceptor heterojunctions, Science 270 (5243) (1995) 1789–1791.
[7] J. Nelson, Polymer:fullerene bulk heterojunction solar cells, Mat. Today 14 (10) (2011) 462–470.
[8] Y.-J. Cheng, S.-H. Yang, C.-S. Hsu, Synthesis of conjugated polymers for organic Solar cell applications, Chem. Rev. 109 (11) (2009) 5868–5923.
[9] S. Günes, H. Neugebauer, N.S. Sariciftci, Conjugated polymer-based organic Solar cells, Chem. Rev. 107 (4) (2007) 1324–1338.
[10] Y. Liu, J. Zhao, Z. Li, C. Mu, W. Ma, H. Hu, K. Jiang, H. Lin, H. Ade, H. Yan, Aggregation and morphology control enables multiple cases of high-efficiency polymer solar cells, Nat. Commun. 5 (2014).
[11] C. Liu, C. Yi, K. Wang, Y. Yang, R.S. Bhatta, M. Tsige, S. Xiao, X. Gong, Single-junction polymer Solar cells with over 10% efficiency by a novel two-dimensional donor–acceptor conjugated copolymer, ACS Appl. Mater. Interfaces 7 (8) (2015) 4928–4935.
[12] T. Yamamoto, Z.-h. Zhou, T. Kanbara, M. Shimura, K. Kizu, T. Maruyama, Y. Nakamura, T. Fukuda, B.-L. Lee, N. Ooba, S. Tomaru, T. Kurihara, T. Kaino, K. Kubota, S. Sasaki, π-conjugated Donor–Acceptor copolymers constituted of π-excessive and π-deficient arylene units. Optical and electrochemical properties in Relation to CT Structure of the polymer, J. Am. Chem. Soc. 118 (43) (1996) 10389–10399.
[13] P.M. Beaujuge, J.M.J. Fréchet, Molecular design and ordering effects in π-functional materials for transistor and Solar cell applications, J. Am. Chem. Soc.

133 (50) (2011) 20009–20029.
[14] Y. Li, Molecular design of photovoltaic materials for polymer Solar cells: toward suitable electronic energy levels and broad absorption, Acc. Chem. Res. 45 (5) (2012) 723–733.
[15] B. Carsten, F. He, H.J. Son, T. Xu, L. Yu, Stille polycondensation for Synthesis of functional materials, Chem. Rev. 111 (3) (2011) 1493–1528.
[16] M. Jeffries-El, B.M. Kobilka, B.J. Hale, Optimizing the performance of conjugated polymers in organic photovoltaic cells by traversing group 16, Macromolecules 47 (21) (2014) 7253–7271.
[17] J.J. Intemann, K. Yao, H.-L. Yip, Y.-X. Xu, Y.-X. Li, P.-W. Liang, F.-Z. Ding, X. Li, A.K.Y. Jen, Molecular weight effect on the absorption, charge carrier mobility, and photovoltaic performance of an indacenodiselenophene-based ladder-type polymer, Chem. Mater. 25 (15) (2013) 3188–3195.
[18] B.M. Kobilka, B.J. Hale, M.D. Ewan, A.V. Dubrovskiy, T.L. Nelson, V. Duzhko, M. Jeffries-El, Influence of heteroatoms on photovoltaic performance of donor–acceptor copolymers based on 2,6-di(thiophen-2-yl)benzo[1,2-b:4,5-b′]difurans and diketopyrrolopyrrole, Polym. Chem. 4 (20) (2013) 5329.
[19] C.H. Woo, P.M. Beaujuge, T.W. Holcombe, O.P. Lee, J.M.J. Fréchet, Incorporation of furan into low band-gap polymers for efficient Solar cells, J. Am. Chem. Soc. 132 (44) (2010) 15547–15549.
[20] J. Hollinger, D. Gao, D.S. Seferos, Selenophene electronics, Isr. J. Chem. 54 (5–6) (2014) 440–453.
[21] J. Ohshita, Conjugated oligomers and polymers containing dithienosilole units, Macromol. Chem. Phys. 210 (17) (2009) 1360–1370.
[22] Y. Zou, A. Najari, P. Berrouard, S. Beaupré, B. Réda Aïch, Y. Tao, M. Leclerc, A thieno[3,4-c]pyrrole-4,6-dione-based copolymer for efficient Solar cells, J. Am. Chem. Soc. 132 (15) (2010) 5330–5331.
[23] T.Y. Chu, J. Lu, S. Beaupre, Y. Zhang, J.R. Pouliot, S. Wakim, J. Zhou, M. Leclerc, Z. Li, J. Ding, Y. Tao, Bulk heterojunction Solar cells using thieno[3,4-c]pyrrole-4,6-dione and dithieno[3,2-b:2′,3′-d]silole copolymer with a power conversion efficiency of 7.3%, J. Am. Chem. Soc. 133 (12) (2011) 4250–4253.
[24] C.M. Amb, S. Chen, K.R. Graham, J. Subbiah, C.E. Small, F. So, J.R. Reynolds, Dithienogermole as a fused electron donor in bulk heterojunction Solar cells, J. Am. Chem. Soc. 133 (26) (2011) 10062–10065.
[25] S. Beaupré, A. Pron, S.H. Drouin, A. Najari, L.G. Mercier, A. Robitaille, M. Leclerc, Thieno-, furo-, and selenopheno[3,4-c]pyrrole-4,6-dione copolymers: effect of the heteroatom on the electrooptical properties, Macromolecules 45 (17) (2012) 6906–6914.
[26] T. Ikai, A.K.M.F. Azam, M. Kuzuba, T. Kuwabara, K. Maeda, K. Takahashi, S. Kanoh, Synthesis of seleno[3,4-c]pyrrole-4,6-dione-based polymers for polymer solar cells, Synth. Met. 162 (17–18) (2012) 1707–1712.
[27] S.K. Pollack, Y.M. Hijji, B. Kgobane, Poly(2-alkylpyrrolo[3.4-c]-1,3-(2H,5H)-dioxopyrrole-4,6-diyl)s. A novel class of intramolecularly hydrogen-bonded, conjugated polymers, Macromolecules 30 (21) (1997) 6709–6711.
[28] V. Tamilavan, M. Song, R. Agneeswari, J.-W. Kang, D.-H. Hwang, M.H. Hyun, Synthesis and photovoltaic properties of donor–acceptor polymers incorporating a structurally-novel pyrrole-based imide-functionalized electron acceptor moiety, Polymer 54 (22) (2013) 6125–6132.
[29] Y. Li, B. Xu, H. Li, W. Cheng, L. Xue, F. Chen, H. Lu, W. Tian, Molecular engineering of copolymers with Donor–Acceptor Structure for bulk heterojunction photovoltaic cells toward high photovoltaic performance, J. Phys. Chem. C 115 (5) (2011) 2386–2397.
[30] O. Ostroverkhova, S. Shcherbyna, D.G. Cooke, R.F. Egerton, F.A. Hegmann, R.R. Tykwinski, S.R. Parkin, J.E. Anthony, Optical and transient photoconductive properties of pentacene and functionalized pentacene thin films: dependence on film morphology, J. Appl. Phys. 98 (3) (2005) 033701.
[31] Y. Zhu, R.D. Champion, S.A. Jenekhe, Conjugated Donor–Acceptor copolymer semiconductors with large intramolecular charge Transfer: Synthesis, optical properties, electrochemistry, and field effect carrier mobility of thienopyrazine-based copolymers, Macromolecules 39 (25) (2006) 8712–8719.
[32] P.M. Beaujuge, C.M. Amb, J.R. Reynolds, Spectral engineering in π-conjugated polymers with intramolecular Donor–Acceptor interactions, Acc. Chem. Res. 43 (11) (2010) 1396–1407.
[33] C. Duan, F. Huang, Y. Cao, Recent development of push-pull conjugated polymers for bulk-heterojunction photovoltaics: rational design and fine tailoring of molecular structures, J. Mater. Chem. 22 (21) (2012) 10416–10434.
[34] C.M. Cardona, W. Li, A.E. Kaifer, D. Stockdale, G.C. Bazan, Electrochemical considerations for determining absolute frontier orbital energy levels of conjugated polymers for solar cell applications, Adv. Mat. 23 (20) (2011) 2367–2371.
[35] L. Zhang, Q. Zhang, H. Ren, H. Yan, J. Zhang, H. Zhang, J. Gu, Calculation of band gap in long alkyl-substituted heterocyclic-thiophene-conjugated polymers with electron donor–acceptor fragment, Sol. Energy Mater. Sol. Cells 92 (5) (2008) 581–587.
[36] C. Møller, M.S. Plesset, Note on an approximation treatment for many-electron Systems, Phys. Rev. 46 (7) (1934) 618–622.
[37] R.M. Osuna, R.P. Ortiz, T. Okamoto, Y. Suzuki, S. Yamaguchi, V. Hernández, J.T. López Navarrete, Thiophene- and Selenophene-based Heteroacenes: combined quantum chemical DFT and spectroscopic Raman and UV–Vis–NIR Study, J. Phys. Chem. B 111 (26) (2007) 7488–7496.
[38] Y. Liang, D. Feng, Y. Wu, S.-T. Tsai, G. Li, C. Ray, L. Yu, Highly efficient Solar cell polymers developed via fine-tuning of Structural and electronic properties, J. Am. Chem. Soc. 131 (22) (2009) 7792–7799.
[39] B. Milián-Medina, J. Gierschner, π-Conjugation, Wiley Interdiscip. Rev. Comput. Mol. Sci. 2 (4) (2012) 513–524.
[40] J.F. Mike, K. Nalwa, A.J. Makowski, D. Putnam, A.L. Tomlinson, S. Chaudhary, M. Jeffries-EL, Synthesis, characterization and photovoltaic properties of poly(thiophenevinylene-alt-benzobisoxazole)s, Phys. Chem. Chem. Phys. 13 (4) (2011) 1338–1344.
[41] C.-K. Tai, C.-A. Hsieh, K.-L. Hsiao, B.-C. Wang, Y. Wei, Novel dipolar 5,5,10,10-tetraphenyl-5,10-dihydroindeno[2,1-a]-indene derivatives for SM-OPV: a combined theoretical and experimental study, Org. Electron. 16 (2015) 54–70.
[42] M. Malagoli, J.L. Brédas, Density functional theory study of the geometric structure and energetics of triphenylamine-based hole-transporting molecules, Chem. Phys. Lett. 327 (1–2) (2000) 13–17.
[43] W.J. Chi, Z.S. Li, The theoretical investigation on the 4-(4-phenyl-4-alpha-naphthylbutadieny)-triphenylamine derivatives as hole transporting materials for perovskite-type solar cells, Phys. Chem. Chem. Phys. 17 (8) (2015) 5991–5998.
[44] C. Sun, D. Qi, Y. Li, L. Yang, Tunable spectra and charge transfer process of benzodifurandione-based polymer by sulfur substitution, RSC Adv. 5 (24) (2015) 18492–18500.